Analysis of 2D CS Spectra for Systems with Non-Gaussian Dynamics

Roy, Santanu; Pshenichnikov, Maxim S.; Jansen, Thomas L. C.

Published in:
Journal of Physical Chemistry B

DOI:
10.1021/jp109742p

Publication date:
2011

THE JOURNAL OF PHYSICAL CHEMISTRY B

ARTICLE

pubs.acs.org/JPCB

Analysis of 2D CS Spectra for Systems with Non-Gaussian Dynamics

Santanu Roy, Maxim S. Pshenichnikov, and Thomas L. C. Jansen*

Zernike Institute for Advanced Materials, University of Groningen, Nijenborgh 4, 9747 AG Groningen, The Netherlands

ABSTRACT: We investigate how accurate different methods of the spectral line shape analysis work in two-dimensional correlation spectroscopy (2D CS) for systems with non-Gaussian dynamics. A direct link is established between the frequency dependent correlation functions and a number of line shape metrics. Two model systems are constructed mimicking a typical molecular system with conventional Gaussian and non-Gaussian spectral dynamics. The frequency dependent correlation function and several line shape parameters extracted from the 2D CS spectra at different waiting times reveal dissimilar dynamics in different frequency domains in the non-Gaussian case and similar dynamics in all domains in the Gaussian case. The extracted frequency dependent correlation times agree well with the local dynamics in the underlying model for all analysis methods. We also find an extension of the existing line shape analysis methods that allows the extraction of the third-order correlation function.

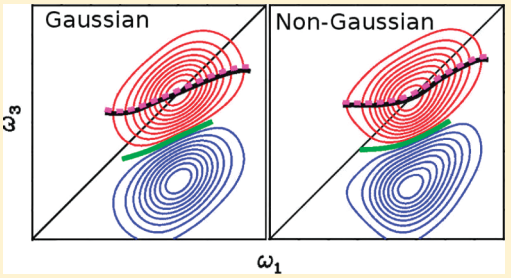

I. INTRODUCTION

Frequency fluctuations of optical transitions in the visible or IR domains have been extensively used in the last decades to obtain information about system dynamics in physics, chemistry, biology, and material sciences. The frequency fluctuation autocorrelation functions can be extracted from third-order nonlinear optical experiments.[1−3] One notable example of such an experiment is the photon echo peak shift.[4,5] The emergence of two-dimensional correlation spectroscopy (2D CS)[6] made it possible to obtain much more detailed information on the frequency fluctuations than the photon echo peak shift. 2D CS is closely related to the well-known two-dimensional NMR COSY technique[7] and basically relies on correlating the frequencies observed at one time with those that are detected after a time delay. In this way the information is spread in two-dimensions and the technique is particularly sensitive to correlations in frequency fluctuations. However, one needs to develop more or less direct methods to analyze the complex two-dimensional lineshapes in an efficient way to extract a wealth of information such as the frequency fluctuation autocorrelation functions from the peak shape.

In such an analysis, the central limit theorem is often used, explicitly or implicitly, to ensure frequency fluctuations have Gaussian dynamics. Therefore, line shapes in linear and nonlinear optical and infrared spectra can be described within the well-known Kubo line shape paradigm of theories,[8−10] also known as the second-order cumulant approximation. We would like to stress, however, that the requirement of Gaussian dynamics is much stronger than simply demanding the frequency distribution to be Gaussian. The latter only requires that the higher-order cumulants are zero for frequencies taken at the same time. In contrast, Gaussian dynamics imply that the higher-order cumulants $\langle\langle\omega(t_1)\cdots\omega(t_n)\rangle\rangle$ $(n > 2)$ are zero for all combinations of the time variables t_i. In other words, a Gaussian frequency distribution or linear absorption line shape does necessarily mean that the underlying dynamics is Gaussian as appears to be a common misconception.

Most 2D CS studies so far have limited themselves to the same basic assumption of Gaussian dynamics for analysis as were used for the photon echo peak shift. Among the suggested metrics, the first moment of the 2D spectrum,[11] using the ellipticity of the peak,[12] the slope of the max-line,[13,14] the nodal slope,[15] and phase slopes[16] are used. The study of the relative intensity between the rephasing and nonrephasing signals denoted the inhomogeneity index is another suggested method for analyzing the two-dimensional spectral peaks.[17] An excellent review for the application of these methods to characterize 2D CS line shapes can be found in ref 17.

For a long time, the only noticeable known exception of non-Gaussian dynamics was chemical exchange systems, which can be accounted for by the Kubo jump models.[8,9] However, recently a number of systems with significant non-Gaussian frequency fluctuations have been found using 2D CS. The first example of non-Gaussian dynamics is the 2D CS spectrum of the OH stretch of water.[18,19] A particular extreme case is H_2O in acetonitrile, where the non-Gaussian dynamics leads to distinctively dissimilar dynamics of the predominantly symmetric and asymmetric OH stretch vibrations.[20] However, non-Gaussian dynamics has also been reported in the optical spectra of light-harvesting complexes of bacteria.[21] Other examples are the 2D CS spectra of the amide I mode of the model peptide unit molecule, *N*-methyl acetamide, in methanol[22,23] and a number of chemical exchange systems.[24−29] Also, three-dimensional (3D IR) spectroscopy[30] has been proposed to probe the deviation

Special Issue: Shaul Mukamel Festschrift

Received: October 11, 2010
Revised: November 29, 2010
Published: January 10, 2011

from Gaussian dynamics directly. A few attempts have been made to perform frequency dependent analysis[31] of experimental spectra mostly focusing on the use of slope analysis;[13,20,32,33] however, the analysis clearly lacked a solid theoretical basis.

In this paper, we investigate how to obtain dynamical information from the 2D spectra of systems with non-Gaussian dynamics. A theoretical connection will be derived between frequency-dependent correlation functions and different metrics. To test the assumptions made in the theory, we set up a model, where the non-Gaussian dynamics is introduced through a frequency dependent friction parameter. Then the numerically calculated 1D and 2D spectra will be subjected to different methods for line shape analysis, and the results will be compared with the frequency-dependent correlation functions obtained directly from the trajectory. This will allow us to assess the reliability of the different line shape analysis methods and justify the application to a broad range of systems that exhibit non-Gaussian dynamics. Finally, we will demonstrate how a higher-order correlation function can be derived from 2D spectra.

The remainder of this paper is organized as follows. In the next section we will describe the theory for inducing the non-Gaussian dynamics in a model system and define different types of frequency fluctuation correlation functions. In Section III we will discuss the methods that we use to calculate 2D CS spectra and introduce the line shape parameters that we will analyze. We will present and discuss the results in Section IV. Finally, we will draw conclusions in Section V.

II. THEORY

In a 2D CS experiment three laser pulses separated by short delay times interact with the sample. t_1 is the delay time between the first two lasers, t_2 is the delay time between the second and third one, known as waiting time, and t_3 is the delay time after the third interaction. The 2D spectrum with the frequency axes ω_1 and ω_3 is obtained by taking the Fourier transform of the time-domain output signal (both real and imaginary parts) with respect to t_1 and t_3. t_2 is kept constant for a spectrum and several spectra with different t_2 are obtained to investigate the underlying waiting time dynamics. The 2D CS signal then consists of the imaginary (absorptive) part of the sum of the rephasing (k_I) and nonrephasing (k_{II}) signals.[34]

A. Construction of the Model System. Let us consider a three level quantum system coupled with a classical harmonic bath. The harmonic bath is again coupled with a Markovian heat bath. Here we assume that the harmonic bath is not affected by the quantum system and that the heat bath is not affected by the harmonic bath. The quantum system is described by the following Hamiltonian.

$$H(t) = [\omega_0 + cx(t)]B^{\dagger}B - \frac{\Delta}{2}B^{\dagger}B^{\dagger}BB \tag{1}$$

The usual Bosonic creation and annihilation operators are denoted $B^{\dagger}$ and B. The average frequency of the singly excited state is ω_0. The magnitude of the coupling to the harmonic bath coordinate, $x(t)$, is determined by the coupling constant c. The anharmonicity is given by the constant Δ.

In order to describe the motion of the harmonic bath a stochastic differential equation, i.e., the Langevin equation, is used.[35]

$$m\frac{d^2x}{dt^2} = -kx - m\gamma(x)\frac{dx}{dt} + F^{\text{heat}} \tag{2}$$

The mass and the harmonic constant are denoted m and k, respectively. The friction connected with the coupling with the heat bath is given by γ. In contrast to the standard Langevin equation the friction is allowed to depend on the coordinate of the harmonic bath, which allows us to introduce non-Gaussian dynamics. The term F^{heat} is a fluctuating random force exerted by the Markovian heat bath and has the following properties:

$$\langle F^{\text{heat}}(t)\rangle = 0 \tag{3}$$

$$\langle F^{\text{heat}}(t)F^{\text{heat}}(0)\rangle = 2\delta(t)\gamma(x(t))mk_BT \tag{4}$$

The essential difference between our harmonic bath and that commonly used is that we use a position dependent friction. We apply the position dependent friction as given bellow:

$$\gamma(x(t)) = \gamma_\sigma[\tanh(\sigma x(t)) + 1]/2 + \gamma_0 \tag{5}$$

This function gives rise to a smooth change between two friction constants (γ_0 and $\gamma_0 + \gamma_\sigma$) that will be found at the extreme values of the bath coordinate. This difference in friction induces the non-Gaussian dynamics. The nonzero values of constant, σ, determine how fast the change between the two domains of friction is. For $\sigma = 0$, the friction is constant, resulting in Gaussian dynamics. The lack of memory in the heat bath ensures that a Gaussian distribution of the bath coordinate is still obtained, even when the friction is not constant. When the characteristic frequency of the harmonic bath coordinate, $\omega_{\text{bath}} = (k/m)^{1/2}$, is low compared with the friction the system is overdamped. In this case one would expect a local correlation function of the harmonic bath coordinate corresponding to that of a Brownian overdamped oscillator that will decay with a bath relaxation time[1] given by

$$\tau_{\text{bath}} = \gamma/{\omega_{\text{bath}}}^2 \tag{6}$$

Later we will choose our parameters so that we are in this overdamped regime.

B. Correlation Functions and Joint Probability Distributions. The frequency autocorrelation function gives the measure of the amplitude and correlation time of the frequency fluctuations. For a given frequency trajectory ($\omega(t)$) the 2nd (C_{11}) and 3rd (C_{21}) order correlation functions are given by the following equations, respectively:

$$C_{11}(t) = \langle(\omega(t) - \langle\omega\rangle)(\omega(0) - \langle\omega\rangle)\rangle \tag{7}$$

$$C_{21}(t) = \langle(\omega(t) - \langle\omega\rangle)^2(\omega(0) - \langle\omega\rangle)\rangle \tag{8}$$

where the brackets denote the ensemble average. $C_{21}(t)$ is interesting as it is the simplest correlation function that vanishes for Gaussian dynamics and its normalized value is a measure of time-dependent skewness. It is possible to extract the correlation functions from the 2D CS spectra in the spectral diffusion limit, i.e. assuming the dynamics to be slow at the time scales of t_1 and t_3 time intervals (but not during the waiting time t_2). In this limit the 2D spectrum of a single mode is determined by the joint probability distribution (JPD) $D(\omega_1, t_2, \omega_3)$, i.e the probability to find ω_1 as the initial frequency and ω_3 as the final frequency after a waiting time t_2. The signal intensity, $S(\omega_1, t_2, \omega_3)$, can then be approximated as the following:

$$S(\omega_1, t_2, \omega_3) = D(\omega_1, t_2, \omega_3) - D(\omega_1, t_2, \omega_3 + \Delta) \tag{9}$$

$D(\omega_1, t_2, \omega_3)$ and $D(\omega_1, t_2, \omega_3 + \Delta)$ correspond to the diagonal peak (stimulated emission and ground state bleaching) and the overtone peak (excited state absorption) of the 2D CS spectrum,

respectively, where Δ is the anharmonicity. If the anharmonicity is large compared to the absorption spectrum width, the JPD can easily be extracted from the spectrum. If the JPD is known one can use it to calculate the frequency dependent correlation functions.[36]

$$C^{S}(\omega_1, t_2) = \frac{\int_{-\infty}^{\infty} D(\omega_1, t_2, \omega_3)(\omega_1 - \langle\omega_1\rangle)(\omega_3 - \langle\omega_3\rangle)\, d\omega_3}{\int_{-\infty}^{\infty} D(\omega_1, t_2, \omega_3)\, d\omega_3} \tag{10}$$

where $\langle\omega_1\rangle$ and $\langle\omega_3\rangle$ are the average values for ω_1 and ω_3, respectively, and the superscript, S, indicates that the correlation function is extracted from a 2D spectrum and thus not mathematically exact. Hence, for $i = 1$ or 3

$$\langle\omega_i\rangle = \frac{\int_{-\infty}^{\infty}\int_{-\infty}^{\infty} D(\omega_1, t_2, \omega_3)\omega_i\, d\omega_1\, d\omega_3}{\int_{-\infty}^{\infty}\int_{-\infty}^{\infty} D(\omega_1, t_2, \omega_3)\, d\omega_1\, d\omega_3} \tag{11}$$

Further integration of eq 10 with respect to ω_1 leads to the normal correlation function.[36]

$$C_{11}^{S}(t_2) = \frac{\int_{-\infty}^{\infty}\int_{-\infty}^{\infty} D(\omega_1, t_2, \omega_3)(\omega_1 - \langle\omega_1\rangle)(\omega_3 - \langle\omega_3\rangle)\, d\omega_1\, d\omega_3}{\int_{-\infty}^{\infty}\int_{-\infty}^{\infty} D(\omega_1, t_2, \omega_3)\, d\omega_1\, d\omega_3} \tag{12}$$

In order to determine whether the correlation function behaves differently (or similarly) in different frequency domains, the total spectrum is divided into a number of domains along the ω_1 axis, and $C_{11}^{S}(t_2)$ is extracted in each domain and then compared with each other. For a particular domain defined as $\omega_1^{i} \le \omega_1 \le \omega_1^{f}$, where ω_1^{i} and ω_1^{f} are the limiting values for ω_1, eq 12 for such interval is

$$C_{11}^{S}(t_2) = \frac{\int_{\omega_1^{i}}^{\omega_1^{f}} d\omega_1 \int_{-\infty}^{\infty} d\omega_3\, D(\omega_1, t_2, \omega_3)(\omega_1 - \langle\omega_1\rangle)(\omega_3 - \langle\omega_3\rangle)}{\int_{-\infty}^{\infty}\int_{-\infty}^{\infty} D(\omega_1, t_2, \omega_3)\, d\omega_1\, d\omega_3} \tag{13}$$

The higher-order correlation functions, for example, the third-order correlation function can also be obtained as the following

$$C_{21}^{S}(t_2) = \frac{\int_{-\infty}^{\infty}\int_{-\infty}^{\infty} D(\omega_1, t_2, \omega_3)(\omega_1 - \langle\omega_1\rangle)(\omega_3 - \langle\omega_3\rangle)^2\, d\omega_1\, d\omega_3}{\int_{-\infty}^{\infty}\int_{-\infty}^{\infty} D(\omega_1, t_2, \omega_3)\, d\omega_1\, d\omega_3} \tag{14}$$

When D is the actual JPD eq 12 and eq 14 are mathematically identical to eqs 7 and 8, respectively. When D is extracted from the spectra, eqs 12 and 14 give extracted correlation functions.

C. Metrics and Their Connection with Correlation Functions. Figure 1 illustrates a number of metrics that will be used to analyze the frequency-dependent dynamics. The antidiagonal width is the full width at half-maximum (fwhm) of a slice along the antidiagonal direction centered at a particular value of ω_1. The max-line slope is the slope of the line obtained by plotting the value of ω_3, where the intensity is the highest for a particular value of ω_1, as a function of ω_1. The phase slope is defined in the following way. The output intensity in the 2D CS experiment has a dispersive (d) and an absorptive (a) part, and the phase is defined as $\tan^{-1}(d/a)$. Initially a point on the diagonal ($\omega_1 = \omega_3 = \Omega$) is chosen to calculate the phase, then a constant phase line with the same phase on the diagonal peak is obtained. Finally, the nodal slope is defined as the slope of the line in the nodal plane between the diagonal and overtone peaks, where the intensity is zero.

The max-line, nodal line, or phase line can be used to extract the second- and third-order correlation functions in an approximate way, by assuming that they are a good measure of the

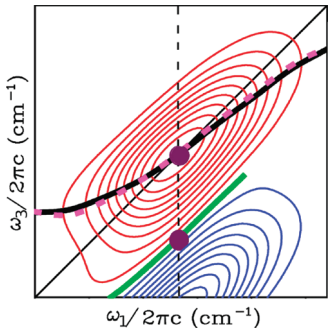

Figure 1. Illustration of different metrics to analyze frequency-dependent dynamics: the max-line (black), phase line (magenta dashed line), and nodal line (green) on the 2D peaks. The intersection points between these lines and the vertical dashed line indicate $\omega_i = \omega_c$, the point of expansion introduced in eq 15.

average final frequency ω_f of the subensemble excited with the initial frequency ω_i apart from a constant, which is independent of the initial frequency. This line is a function, $\omega_f(\omega_i)$, which can be expanded into Taylor series around a point ω_c.

$$\omega_f(\omega_c + \Delta\omega) = \omega'_f(\omega_c)\Delta\omega + \frac{1}{2}\omega''_f(\omega_c)(\Delta\omega)^2 + O(\Delta\omega^3) \tag{15}$$

Here, we cut the series beyond the second-order term. $\omega'_f(\omega_c) = (d\omega_f(\omega_i)/d\omega_i)|_{\omega_i=\omega_c}$ and $\omega''_f(\omega_c) = (d^2\omega_f(\omega_i)/d\omega_i^2)|_{\omega_i=\omega_c}$ are the slope and curvature, respectively, at the point of expansion, ω_c. Considering the Gaussian distribution, $D(\omega_c + \Delta\omega) = [1/(2\pi\sigma^2)^{1/2}] \exp(-\Delta\omega^2/2\sigma^2)$, we obtain the correlation functions as

$$\begin{aligned} C_{11}^{S}(t, \omega_c) &= \int_{-\infty}^{\infty} \Delta\omega\omega_f(\omega_c + \Delta\omega)D(\omega_c + \Delta\omega)\, d(\Delta\omega) \\ &= \sigma^2\omega'_f(\omega_c) + O(\Delta\omega^4) \end{aligned} \tag{16}$$

$$\begin{aligned} C_{21}^{S}(t, \omega_c) &= \int_{-\infty}^{\infty} (\Delta\omega)^2\omega_f(\omega_c + \Delta\omega)D(\omega_c + \Delta\omega)\, d(\Delta\omega) \\ &= (3/2)\sigma^4\omega''_f(\omega_c) + O(\Delta\omega^6) \end{aligned} \tag{17}$$

$C_{11}^{S}(t,\omega_c)/\sigma^2$ and $C_{21}^{S}(t,\omega_c)/\sigma^3$ are the normalized second and third-order correlation functions, respectively, and we have used that $\sigma = \int_{-\infty}^{\infty}\Delta\omega\Delta\omega D(\omega_c + \Delta\omega)\, d(\Delta\omega)$. The argument ω_c emphasizes that the correlation functions are obtained by an expansion around that particular point. In practice, we will consider a region of the spectral range (as will be defined later) with ω_c in the center of this domain, and the slope and curvature will be calculated at each point of this domain by calculating finite differences between neighboring points. We then average over all points within the domain to obtain the final slope and curvature.

III. METHODS

A Hamiltonian trajectory was constructed by numerical propagation of eq 2 with snapshots stored every 10 fs for a total time interval of 400 ns. The values for all parameters used to construct the trajectory are listed in Table 1. Note that the central

dx.doi.org/10.1021/jp109742p |J. Phys. Chem. B 2011, 115, 5431–5440

Table 1. Values for All Parameters Used in the Simulation

parameters	values
k	10 (kJ/mol/nm^2)
m	20 (u)
γ_0	0.1×10^{-3} (fs^{-1})
σ	2 (nm^{-1})
γ_σ	0.3×10^{-3} (fs^{-1})
T	300 (K)
c	100 (cm^{-1}/nm)
ω_0	1050 (cm^{-1})
Δ	150 (cm^{-1})

frequency is our arbitrarily choice, and the model can be readily rescaled to any other frequencies, for instance, visible or UV. Linear absorption and 2D CS spectra were calculated from this trajectory by solving the time-dependent Schrödinger equation using the numerical integration of Schrödinger equation scheme (NISE).[37,38] In this scheme, the total time is divided into a number of short time intervals (10 fs) and we treat the Hamiltonian as constant for the short time intervals and during each time interval the time independent Schrödinger equation is solved. The successive propagation in these short time intervals is used to get the time evolution for the total time. The linear and nonlinear response functions are then calculated to get the linear absorption and 2D CS spectra.

For the purpose of analyzing the lineshapes of the 2D CS spectra, we calculate the antidiagonal width and max-line slope, phase slope, and nodal slope. To do this we obtain the diagonal peak in two ways. First, we consider only the positive part of the spectrum which gives the diagonal peak influenced by the interference with the negative peak. We call this the actual spectrum. Second, a positive signal is added to the spectrum for each ω_1 in the decreasing direction of ω_3 when $\omega_3 > \omega_3^{\text{initial}} + \Delta$, assuming the positive diagonal peak and the negative overtone peak are equal. In other words, we trust the signal until $\omega_3^{\text{initial}} + \Delta$ and then correct the rest part by adding a positive signal which essentially eats up the negative part. Thus, we obtain a corrected spectrum on the diagonal without the influence from the interference. We call this the corrected spectrum. Such a treatment is only valid when the dynamics determining the two peaks are the same and the anharmonicity is frequency independent. The diagonal peaks obtained in both ways are subjected to the calculation of antidiagonal width, max-line slope and phase slope.

IV. RESULTS AND DISCUSSION

All of the calculations were performed for two cases. First is the Gaussian case where a constant friction (0.25×10^{-3} fs^{-1}) is considered. Using eq 6 and the parameters listed in Table 1, the correlation time of the bath dynamics for this case turns out to be 500 fs. Second is the non-Gaussian case where the friction is changing smoothly between 0.1×10^{-3} and 0.4×10^{-3} fs^{-1} as a function of the harmonic bath coordinate, i.e., the time scale of the bath dynamics is between 200 and 800 fs.

For both cases we present a comparison between the distribution of frequencies calculated from the frequency trajectory and the calculated linear absorption spectrum in Figure 2. Both the distributions and the linear absorption spectra are centered at the average frequency, $\langle\omega\rangle$ = 1050 cm^{-1}. The almost perfect overlapping of the linear absorption spectrum with the frequency distribution reveals that motional narrowing is practically negligible;

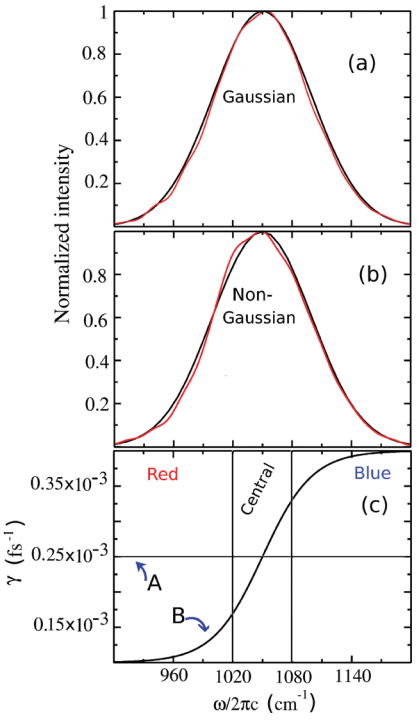

Figure 2. The linear absorption spectra (red) and frequency distributions (black) for the Gaussian case (a) and non-Gaussian case (b). (c) The relation between the friction and frequency for the Gaussian (A) and non-Gaussian case (B). The whole frequency domain is divided into three subdomains: red, central, and blue.

that is, we fulfill the assumption of the spectral diffusion limit discussed previously. It should be realized that the linear spectra both in the Gaussian case and the non-Gaussian case have a practically perfect Gaussian line shape determined by the underlying Gaussian frequency distribution, $D(\omega)$, which is dictated by the Boltzmann distribution of the harmonic bath coordinate

$$D(\omega) = \exp\left[-\frac{-\frac{1}{2}k(\omega/c)^2}{k_B T}\right] \quad (18)$$

For analysis purposes we will define three frequency domains: red domain ($\omega \leq 1020$ cm^{-1}), central domain (1020 cm^{-1} $< \omega <$ 1080 cm^{-1}), and blue domain ($\omega \geq 1080$ cm^{-1}). A direct correspondence between the frequency and the friction (eq 1 and eq 5) is depicted in Figure 2. We chose these domains such that for the non-Gaussian case, the red and blue domains correspond to the domains of small and large friction, respectively, whereas the friction is independent of frequency for the Gaussian case.

A. 2D CS and Correlation Functions. The 2D CS spectra were calculated for both the Gaussian and non-Gaussian case with waiting times spaced by 100 fs, from t_2 = 0 to 2000 fs. The representative 2D spectra at several waiting times are shown in Figure 3. For both the cases, for t_2 = 0 fs, the peaks in the 2D spectrum are diagonally elongated and as the waiting time increases the spectrum starts to spread in the antidiagonal direction. The peaks at longer waiting times aquire a round shape. This is due to the fact that the correlation between the pump and probe frequencies is lost for the longer waiting time. One way to quantify how fast this correlation decays is to extract the correlation function ($C_{11}^{S}(t_2)$) from the spectra as defined in eq 12. For this

dx.doi.org/10.1021/jp109742p |J. Phys. Chem. B 2011, 115, 5431–5440

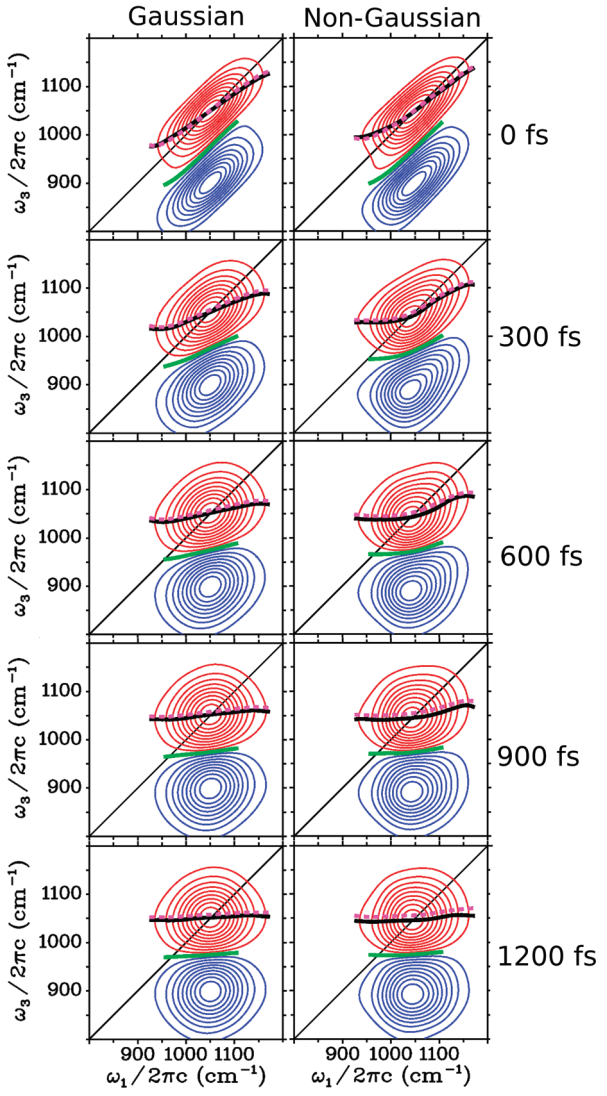

Figure 3. 2D CS spectra at different delay times for the non-Gaussian and Gaussian case. A total of 18 equally spaced contours are plotted between ±10% and ±90% of the most intense peak. Black, magenta, and green lines indicate max-line, phase, and nodal slopes, respectively.

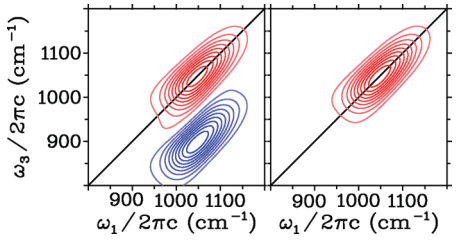

Figure 4. Removal of the overtone peak from a 2D CS spectrum: obtaining a corrected spectrum.

purpose we obtain the actual spectrum and the corrected spectrum as described in Section III. An example of the corrected spectrum is depicted in Figure 4.

We calculate $C_{11}^{S}(t_2)$ for each spectral domain (eq 13) and also for the whole spectrum (red + central + blue) and compare with $C_{11}(t)$ (eq 7) calculated directly from the frequency trajectory in Figure 5 and 6. To calculate $C_{11}^{S}(t_2)$ we employed the frequency

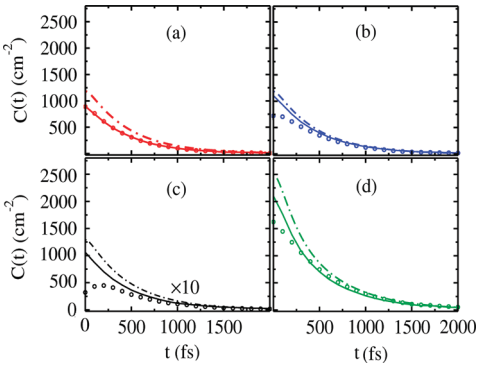

Figure 5. The correlation functions for the Gaussian case for the red domain (a), blue domain (b), central domain (c), and total spectrum (d). The dash-dotted lines, full lines, and circles correspond to the frequency trajectory, corrected spectra, and actual spectra, respectively. The correlation functions in the central domain (c) are scaled with a factor of 10.

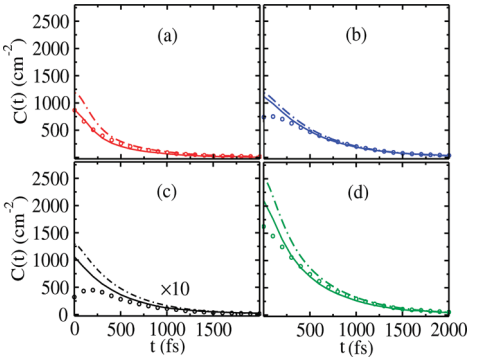

Figure 6. Same as Figure 5 but for the non-Gaussian case.

averages obtained from spectra calculated at t_2 = 1800 fs. This ensures that the extracted correlation functions decay to zero at long times. Summation of the correlation functions from the red, blue and central domains gives the total correlation function of the whole domain. The central domain contributes very little to the total correlation function. This is because the initial value of the frequency is bound to be close to the average in this domain value always resulting in a small value of the product in the correlation function. For the non-Gaussian case (Figure 6), the correlation function decays faster in the red domain than in the blue domain, because the frequency fluctuation is faster in the red domain. For each of the domains, the initial value of the correlation function calculated from the frequency trajectory ($C_{11}(0)$) is greater than that extracted from the spectrum ($C_{11}^{S}(0)$). This reflects the motional narrowing caused by the dynamics during t_1 and t_3. The long time behavior of $C_{11}^{S}(t_2)$ is found to be the same as of $C_{11}(t)$. For the Gaussian case motional narrowing is also observed (Figure 5), and the correlation functions in the red and blue domain display similar dynamics.

$C_{11}(t)$ in the red and blue domain for both the Gaussian and the non-Gaussian case are presented in Figure 7. In the Gaussian case the correlation functions on the red and the blue side are identical up to 1500 fs where differences are observed due to the limited sampling. For the non-Gaussian case, the correlation function at the red side initially decays faster than that on the blue side. However, at times longer than 500 fs the red domain correlation function decay with the same rate as the blue domain

dx.doi.org/10.1021/jp109742p |J. Phys. Chem. B 2011, 115, 5431–5440

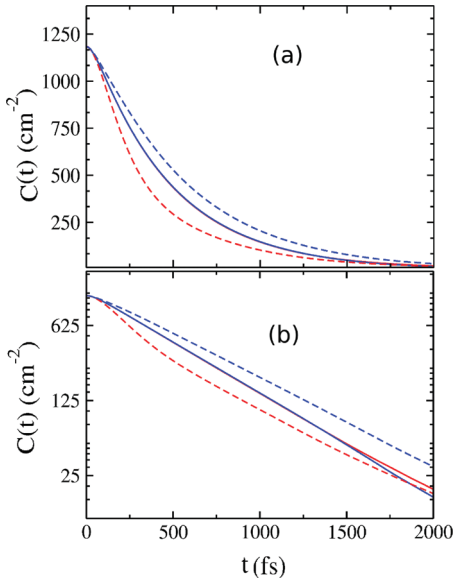

Figure 7. Correlation functions calculated from the frequency trajectory in the linear (a) and (b) logarithmic scale in the red (red line) and blue (blue line) domain for the Gaussian (full line) and non-Gaussian case (dashed line). For the Gaussian case the blue line overlaps with the red line.

correlation function. At this time the correlation functions are determined by the slowest motion found at the blue side. For the non-Gaussian case, the time scale of the dynamics in the blue and middle domain were found by fitting the correlation functions to a monoexponential function $C(t) = A\exp(-t/\tau)$, while in the red domain we used a biexponential function $[C(t) = A\exp(-t/\tau) + B\exp(-t/\tau_{blue})]$ where the value for τ_{blue} extracted from the fitting in the blue domain is used. For the Gaussian case, all the correlation functions were fitted to the monoexponential function. The correlation times, τ, for the all the correlation functions are given in Table 2. For the non-Gaussian case, the correlation times calculated directly from the frequency trajectory are very close to those extracted from the corrected spectra. It is observed in both red and blue domain that the dynamics predicted for $C^S_{11}(t_2)$ from the actual spectra is slower than the dynamics predicted for $C^S_{11}(t_2)$ from the corrected spectra. Obviously, it turns out that the red domain (τ_{red} is 250−300 fs) is involved in faster dynamics than the blue domain (τ_{blue} is 550−700 fs). In the Gaussian case, the correlation times are more or less same ($\tau \sim 470$ fs) with an exception for that calculated in the blue domain of the actual spectra.

B. Line Shape Analysis. The max-line, nodal, and phase slopes and antidiagonal width are line shape parameters which can be useful to investigate quantitatively how the shape of the 2D CS spectrum changes as the waiting time increases and learn about the underlying dynamics. For both the non-Gaussian and Gaussian case the max-line and phase curve lines for the actual spectra and the nodal curve lines at all waiting times are presented in Figure 3. As the waiting time increases, for the non-Gaussian case these curve lines are rotating faster toward a horizontal orientation on the red side than the blue side of the 2D CS spectrum, whereas for the Gaussian case these are rotating simultaneously in the two domains. For each spectrum we calculated the average max-line and nodal slope in the range for which ω_1 is between 1000 and 1020 cm^{-1} in red domain and between 1080 and 1100 cm^{-1} in the blue domain. To calculate

Table 2. Correlation Times in the Dynamics for the Non-Gaussian and Gaussian Case[a]

non-Gaussian case	τ_{red} (fs)	$\tau_{central}$ (fs)	τ_{blue} (fs)
$C_{11}(t)$	255		560
$C^S_{corrected}(t_2)$	285		565
$C^S_{actual}(t_2)$	320		730
max-line slope$_{corrected}$	195	505	750
max-line slope$_{actual}$	190	530	750
nodal slope	205	425	560
phase slope$_{corrected}$	220	530	745
phase slope$_{actual}$	205	515	710
gaussian case	τ_{red} (fs)	$\tau_{central}$ (fs)	τ_{blue} (fs)
$C_{11}(t)$	470		470
$C^S_{corrected}(t_2)$	460		480
$C^S_{actual}(t_2)$	465		575
max-line slope$_{corrected}$	540	500	500
max-line slope$_{actual}$	550	505	500
nodal slope	415	435	465
phase slope$_{corrected}$	505	495	500
phase slope$_{actual}$	500	490	500

[a] The subscripts, corrected and actual, stand for the corrected and actual spectra, respectively.

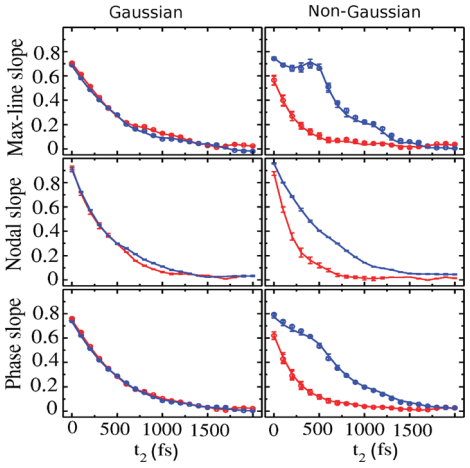

Figure 8. Variation of max-line, nodal, and phase slopes as a function of waiting time: red and blue lines stand for the red and blue domains. Circles correspond to the actual spectra, whereas, the full lines correspond to the corrected spectra. The vertical lines are the error bars.

the phase slope, first we chose a point, $\omega_1 = \omega_3 = 1050$ cm^{-1}, in the center of spectrum at $t_2 = 0$ fs, and a constant phase line with the phase calculated at this point is obtained. The average slope of this constant phase line was calculated using the same range for ω_1 in the red and blue domain as done for the other slopes. The decay of the average max-line, nodal, and phase slopes as a function of waiting time for the non-Gaussian and Gaussian case are depicted in Figure 8. The average max-line slopes for both corrected and actual spectra overlap with each other. We observe the same for the phase slopes as well. For the non-Gaussian case faster decay of the different slopes in the red domain than in the blue domain clearly separates the dynamics with different time scales, i.e., dissimilar dynamics in the red and blue domain. For the Gaussian case, in the decay of the different slopes similar

dx.doi.org/10.1021/jp109742p |J. Phys. Chem. B 2011, 115, 5431–5440

Table 3. Fitted Correlation Times Corresponding to Different Frequencies (ω_1) Exctracted from the Antidiagonal Width for the Non-Gaussian and Gaussian Case[a]

ω_1 (cm^{-1})	$\tau_{corrected}$ (fs)	τ_{actual} (fs)
	Non-Gaussian Case	
1010	245	150
1050	440	470
1090	665	690
	Gaussian Case	
1010	435	415
1050	430	455
1090	465	475

[a] $\tau_{corrected}$ and τ_{actual} indicate the correlation times for the corrected and actual spectra, respectively.

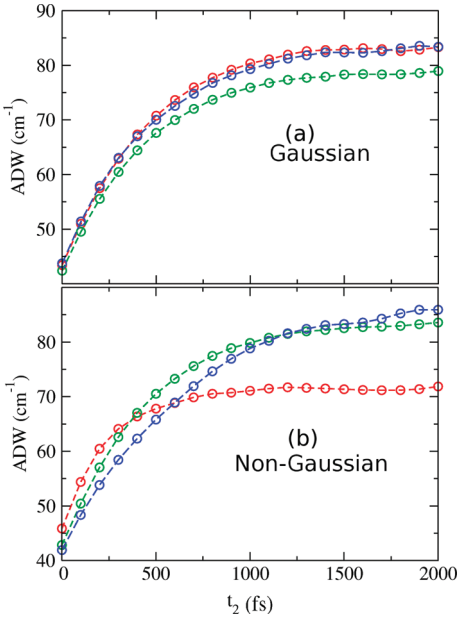

Figure 9. Time evolution of the antidiagonal widths calculated from the corrected spectra for the Gaussian and non-Gaussian case. Red, green, and blue stand for different values of ω_1, i.e., 1020, 1050, and 1090 cm^{-1}, respectively.

dynamics are observed in both domains. To quantify how fast these slopes decay we follow here the same fitting procedure as we did for the correlation functions. The fitted correlation times are given in Table 2. For the non-Gaussian case, the fitted correlation times corresponding to these slopes are in the range 190−220 fs in the red domain and in the range 550−750 fs in the blue domain. For the Gaussian case, these are clustered around 500 fs.

The antidiagonal widths (see Method section) of the corrected and the actual spectra for all waiting times corresponding to different frequencies (Table 3) were calculated. In Figure 9 the time dependent exponential behavior of the antidiagonal widths of the corrected spectra is depicted. The following function is used to extract the corresponding correlation times.

$$\Gamma = \Gamma_a - \Gamma_b \exp(-t/\tau) \qquad (19)$$

These fitted times scales for the antidiagonal widths are listed in Table 3. From this table and Figure 9 it is clear that the

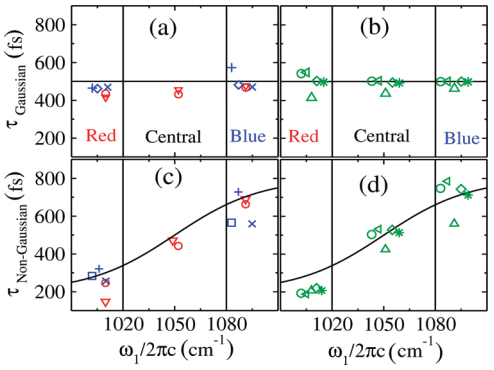

Figure 10. Correlation times for the Gaussian (a and b) and non-Gaussian (c and d) dynamics. The black lines are τ_{bath}. The other correlation times are calculated from the antidiagonal width (red triangle and circle for the actual and corrected spectra, respectively), correlation functions (blue cross, box, and plus indicate values obtained from frequency trajectory, corrected spectra, and actual spectra, respectively), max-line slopes (green circle and triangle pointing left, respectively), nodal slope (green triangle pointing up), and phase slope (green diamonds and star for the corrected and actual spectra, respectively.).

antidiagonal width does reflect the dissimilar dynamics in different frequency domains for the non-Gaussian case and the similar dynamics in all frequency domains for the Gaussian case.

In Figure 10 we give a summary of the correlation times extracted from all the correlation functions and spectral line shape parameters, as compared to the correlation time for the dynamics of the harmonic bath (τ_{bath}). The purpose is to examine to what extend the different metrics provide a correct estimation of the local dynamics. Revisiting eq 6, for the Gaussian case we find, τ_{bath} = 500 fs, in all domains. In this case (Figure 10a and 10b), the correlation times calculated from all the spectral analysis fluctuate around the constant, τ_{bath} = 500 fs and all of the analysis tool show almost similar accuracy. For the non-Gaussian case the following is observed. The correlation times calculated from the correlation functions separate the dynamics of the red domain from the blue domain, but these calculated from the frequency trajectory and the corrected spectra are slightly underestimated with respect to τ_{bath} in the blue domain (Figure 10c). The correlation times corresponding to the nodal slopes show a good agreement with τ_{bath} in the red and central domain and a slight under estimation in the blue domain. The dynamics predicted from the decay of the max-line slopes in the red, central, and blue domain also show a good agreement with the dynamics of the harmonic bath. The correlation times corresponding to the phase slopes show the best match with the τ_{bath} in all domains. Both for the Gaussian and non-Gaussian case (Figure 10a and 10c) the correlation times corresponding to the antidiagonal widths are very close to τ_{bath}, with slight underestimation for the actual spectra in the red domain for the non-Gaussian case.

The third-order frequency correlation function (eqs 8 and 14) shown in Figure 11 can also be used to distinguish the dynamics between the Gaussian and non-Gaussian cases. $C_{21}(t)$ calculated for the Gaussian case vanishes at all times. For the non-Gaussian case $C_{21}(t)$ is also zero initially, then it increases and reaches maximum at 370 fs and then decreases to zero. $C^S_{21}(t_2)$ extracted from the corrected spectra shows similar features as $C_{21}(t)$ for both the Gaussian and non-Gaussian case. For the actual spectra, $C^S_{21}(t_2)$, starts with positive values for both cases and goes to zero at longer time. The deviation for the corrected spectra is caused

dx.doi.org/10.1021/jp109742p |J. Phys. Chem. B 2011, 115, 5431–5440

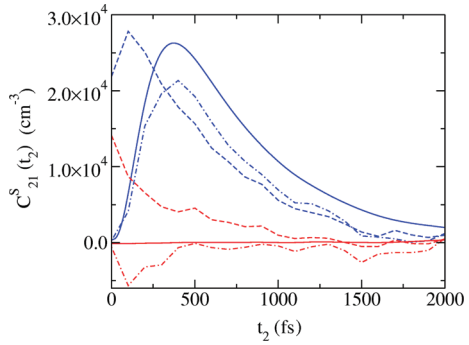

Figure 11. Third order time correlation function calculated for the Gaussian (red) and non-Gaussian (blue) case. Full, dash-dotted, and dashed lines correspond to the frequency trajectory, corrected spectra, and actual spectra, respectively.

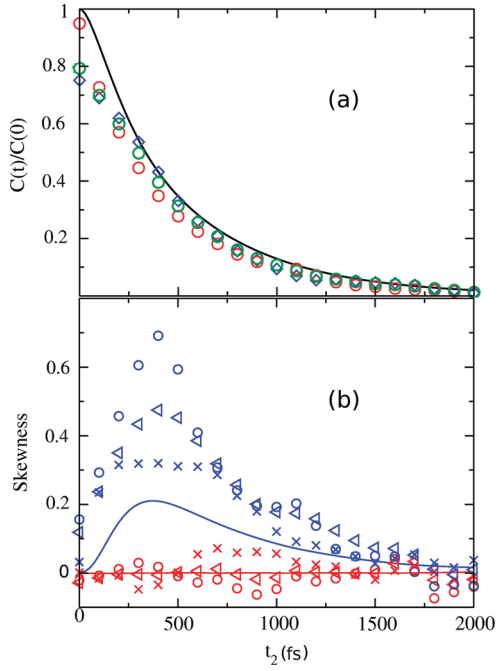

Figure 12. (a) Normalized second-order correlation function calculated from the max-line slope (blue diamond), nodal slope (red circle), and phase slope (green circle) for the actual spectra and compared with that from frequency trajectory (black line). (b) Skewness calculated directly from the frequency trajectory (full lines) for the Gaussian (red) and non-Gaussian (blue) case are compared with those extracted from max-line (circles), phase line (triangles), and nodal line (crosses) curvatures.

by the fact that the contribution from the wings of the spectrum is large and the metric is sensitive to undersampling. For the actual spectra the effect of the interference with the overtone induce an artificial skewness. This shows that higher order-correlation function can be expected to be very challenging to extract from the actual 2D CS spectra in this way provided that there is interference with the overtone. For the corrected spectra the estimate works reasonably well.

In Section III it was shown that the normalized second-order correlation functions can approximately be estimated from the slope extracted from the maxline, nodal line or phase line. We compare these from the actual spectra with the normalized correlation function and skewness calculated directly from the frequency trajectory in the Figure 12a. There is an excellent agreement between the normalized second-order correlation function and the decay curve of the slopes apart from the slightly lower initial values for the slopes due to motional narrowing.

We have also shown that the normalized third-order correlation function, i.e., the time-dependent skewness $C_{21}(t)/\sigma^3$ is proportional to the curvature (eq 17). The agreement between the skewness calculated from the frequency trajectory and curvature for the Gaussian and non-Gaussian case is also reasonably good (Figure 12 b). At short times there is no memory loss on either side and the initial distribution was symmetric so the skewness is zero. At longer times the skewness is essentially the (normalized) difference between the blue side and the red side correlation functions (Figure 7). When the red side loses memory faster, the skewness starts growing to reach its maximum value of 0.21 at the waiting time of 370 fs. At even longer times the skewness decays because the memory is lost on both sides of the spectrum.

Note that the skewness estimated for the non-Gaussian case from the curvature are systematically overestimated. This deviation can be due to the fact that the skewness from the trajectory covers the whole frequency domain, whereas the skewness from the average curvature was calculated in the central domain only. In other words, the higher-order derivatives neglected in eq 17 contribute for our choice of the friction dependence. Nonetheless, the qualitative behavior of the skewness is reconstructed reasonably well.

In recent studies of 3D IR spectroscopy it was found that the full two time third-order correlation function[39]

$$C_3(t_1, t_2) = \langle \omega(t_2)\omega(t_1)\omega(0)\rangle \qquad (20)$$

at least for the OH stretch in liquid water primarily depends on the total population time. Therefore the full third-order correlation function can be approximated by the simpler single time correlation function that we find from the 2D CS phase-line curvatures

$$C_3(t_1, t_2) \approx \langle \omega^2(t_2)\omega(0)\rangle = C_{21}(t_2) \qquad (21)$$

Of course the 3D IR experiment[30] depends on the full three-time third-order correlation function and thus potentially provides more information. Despite recent efforts[30,39−41] unraveling this dynamic information from 3D IR experiments still remain largely an open challenge.

V. CONCLUSION

We have investigated a quantum system coupled with a harmonic bath with frequency dependent friction, which is again coupled with a heat bath, and we have treated the same system, but with a constant friction for the purpose of comparison. We showed that in the spectral diffusion limit a Gaussian linear absorption spectrum was obtained in both cases. This illustrates what appears to be a common misconception that a Gaussian frequency distribution warrants the underlying dynamics to be Gaussian. The strict definition of Gaussian dynamics is that all time-dependent cumulants of higher than second-order are zero. In turn, Gaussian dynamics does ensure a Gaussian frequency distribution.

For both the Gaussian and the non-Gaussian case, we have tested several methods to extract the correlation times from 2D CS spectra. The two point correlation functions calculated from the frequency trajectory and extracted from the 2D CS spectra (corrected and actual spectra) turn out to be extremely useful for

obtaining information about the correlation times in the red and blue domains. For the Gaussian case the predicted correlation times from these correlation functions agree very well with the underlying dynamics of the bath. For the non-Gaussian case the correlation functions do show the difference between the dynamics in the red domain (faster dynamic) and the dynamics in the blue domain (slower dynamics), and corresponding correlation times show a good agreement with the bath relaxation time. The second-order correlation functions extracted from the corrected spectra give the same correlation times as those calculated directly from the frequency trajectory, but differ in the amplitude of the frequency fluctuation due to the motional narrowing. Hence, practically, the second-order correlation function can be extracted from the corrected spectra with correct correlation times, but with underestimation in the initial value. We have also constructed the third-order correlation function from the corrected spectra that appeared to be in good agreement with that calculated from the frequency trajectory. We have shown that within the spectral diffusion limit second and third-order correlation functions can be extracted from the slope and curvature, respectively, at the center of the 2D spectra from the max-line, nodal line or phase line.

The spectral line shape parameters, i.e., the max-line slope, nodal slope, phase slope, and antidiagonal width reveal the correlation times in the red, blue, and central domain, which clearly distinguish the non-Gaussian dynamics from the Gaussian dynamics in good agreement with the known local dynamics. We found that the analysis of the antidiagonal width is an excellent tool to extract the correlation times of the dynamics for a particular frequency. Hence, given 2D CS spectra at different delay times, one will be able to extract the correlation times of the involved dynamics as a function of the frequency by measuring the antidiagonal width. One can track whether the dynamics is similar or dissimilar in the different frequency domains and extract the corresponding correlation times by analyzing the phase, nodal or max-line slopes in these domains.

In real experiments a number of other effects that we have presently not accounted for might complicate the analysis. One of those is finite pulse duration that is always present in experiments. This might lead to the wrong mapping of the real absorption spectrum onto the ω_1/ω_3 axis thereby distorting the analysis. Another potential complication is non-Condon effects that are known to be quite important for the OH stretch of water.[42] It is still an open question how these effects will affect the analysis of the spectral lineshapes. In cases where these effects are large numerical simulations will be needed for interpreting the spectra.

■ ACKNOWLEDGMENT

The authors gratefully thank Shaul Mukamel for numerous fruitful discussions and inspiration. Sean Garrett-Roe and Peter Hamm are gratefully acknowledged for providing the manuscript of their paper (ref 39) prior to publication and for many helpful discussions. T.L.C.J. acknowledges The Netherlands Organization for Scientific Research (NWO) for support through a VIDI grant.

■ REFERENCES

(1) Mukamel, S. *Principles of Nonlinear Optical Spectroscopy*; Oxford University Press: New York, 1995.
(2) Venkatramani, R.; Mukamel, S. *J. Chem. Phys.* **2002,** *117*, 11089.
(3) Cho, M. *Two-dimensional Optical Spectroscopy*; CRC Press: Boca Raton, FL, 2009.
(4) de Boeij, W. P.; Pshenichnikov, M. S.; Wiersma, D. A. *Chem. Phys. Lett.* **1996,** *253*, 53.
(5) Cho, M.; Yu, J.-Y.; Joo, T.; Nagasawa, Y.; Passino, S. A.; Fleming, G. R. *J. Phys. Chem.* **1996,** *100*, 11944.
(6) Hamm, P.; Lim, M. H.; Hochstrasser, R. M. *J. Phys. Chem. B* **1998,** *102*, 6123.
(7) Ernst, R. R.; Bodenhausen, G.; Wokaun, A. *Principles of nuclear magnetic resonance in one and two dimensions* (Oxford University Press, New York, 1995).
(8) Kubo, R. In *Stochastic Processes in Chemical Physics*; Shuler, K. E., Ed.; John Wiley and Sons: New York, 1969; Vol. XV of Adv. Chem. Phys., p 101.
(9) Tanimura, Y. *J. Phys. Soc. Jpn.* **2006,** *75*, 082001.
(10) Mukamel, S. *Phys. Rev. A* **1983,** *28*, 3480.
(11) Gale, G. M.; Gallot, G.; Hache, F.; Lascoux, N.; Bratos, S.; Leicknam, J.-C. *Phys. Rev. Lett.* **1999,** *82*, 1068.
(12) Lazonder, K.; Pshenichnikov, M. S.; Wiersma, D. A. *Opt. Lett.* **2006,** *31*, 3354.
(13) Kraemer, D.; Cowan, M. L.; Paarmann, A.; Huse, N.; Nibbering, E. T. J.; Elsaesser, T.; Miller, R. J. D. *Proc. Natl. Acad. Sci.* **2008,** *105*, 437.
(14) Kwak, K.; Rosenfeld, D. E.; Fayer, M. D. *J. Chem. Phys.* **2008,** *128*, 204505.
(15) Kwac, K.; Cho, M. H. *J. Chem. Phys.* **2003,** *119*, 2256.
(16) Eaves, J. D.; Loparo, J. J.; Fecko, C. J.; Roberts, G. M.; Tokmakoff, A.; Geiger, L. C. *Proc. Natl. Acad. Sci.* **2005,** *102*, 13019.
(17) Roberts, S. T.; Loparo, J. J.; Tokmakoff, A. *J. Chem. Phys.* **2006,** *125*, 084502.
(18) Fecko, C. J.; Eaves, J. D.; Loparo, J. J.; Tokmakoff, A.; Geissler, P. L. *Science* **2003,** *301*, 1698.
(19) Steinel, T.; Asbury, J. B.; Corcelli, S. A.; Lawrence, C. P.; Skinner, J. L.; Fayer, M. D. *Chem. Phys. Lett.* **2004,** *386*, 295.
(20) Jansen, T. L. C.; Cringus, D.; Pshenichnikov, M. S. *J. Phys. Chem. A* **2009,** *113*, 6260.
(21) van Mourik, F.; Chergui, M.; van der Zwan, G. *J. Phys. Chem. B* **2001,** *105*, 9715.
(22) Kwac, K.; Lee, H.; Cho, M. *J. Chem. Phys.* **2004,** *120*, 1477.
(23) DeCamp, M. F.; DeFlores, L.; McCracken, J. M.; Tokmakoff, A.; Kwac, K.; Cho, M. *J. Phys. Chem. B* **2005,** *109*, 11016.
(24) Jansen, T. L. C.; Knoester, J. *J. Chem. Phys.* **2007,** *127*, 234502.
(25) Kim, Y. S.; Hochstrasser, R. M. *Proc. Natl. Acad. Sci.* **2005,** *102*, 11185.
(26) Sanda, F.; Zhuang, W.; Jansen, T. L. C.; Hayashi, T.; Mukamel, S. In *Ultrafast XV*; Corkum, P., Jonas, D. M., Miller, R. J. D., Eds.; Springer: New York, 2006; Vol. 88 of Springer series in chemical physics; p 401.
(27) Scheurer, C.; Steinel, T. *ChemPhysChem* **2007,** *8*, 503.
(28) Cahoon, J. F.; Sawyer, K. R.; Schlegel, J. P.; Harris, C. B. *Science* **2008,** *319*, 1820.
(29) Zheng, J.; Kwak, K.; Asbury, J. B.; Chen, X.; Piletic, I. R.; Fayer, M. D. *Science* **2005,** *309*, 1338.
(30) Garrett-Roe, S.; Hamm, P. *J. Chem. Phys.* **2008,** *128*, 104507.
(31) Møller, K. B.; Rey, R.; Hynes, J. T. *J. Phys. Chem. A* **2004,** *108*, 1275.
(32) Loparo, J. J.; Roberts, S. T.; Tokmakoff, A. *J. Chem. Phys.* **2006,** *125*, 194522.
(33) Bakulin, A. A.; Liang, C.; Jansen, T. L. C.; Wiersma, D. A.; Bakker, H. J.; Pshenichnikov, M. S. *Acc. Chem. Res.* **2009,** *42*, 1229.
(34) Khalil, M.; Demirdoven, N.; Tokmakoff, A. *J. Phys. Chem. A* **2003,** *107*, 5258.
(35) Billing, G. D.; Mikkelsen, K. V. *Introduction to Molecular Dynamics and Chemical Kinetics*; John Wiley & Sons: New York, 1996.
(36) Hamm, P. *J. Chem. Phys.* **2006,** *124*, 124506.
(37) Jansen, T. L. C.; Knoester, J. *J. Phys. Chem. B* **2006,** *110*, 22910.
(38) Jansen, T. L. C.; Knoester, J. *Acc. Chem. Res.* **2009,** *42*, 1405.

(39) Garrett-Roe, S.; Perakis, F.; Hamm, P. 2011, in press.
(40) Garrett-Roe, S.; Hamm, P. *J. Chem. Phys.* **2009,** *130,* 164510.
(41) Garrett-Roe, S.; Hamm, P. *Acc. Chem. Res.* **2009,** *42,* 1412.
(42) Schmidt, J. R.; Corcelli, S. A.; Skinner, J. L. *J. Chem. Phys.* **2005,** *123,* 044513.